INL/CON-23-75479-Revision-0

Investigating Oscillations in Bulb Turbine Plant During Islanded black start Operation

October 2024

Soumyadeep Nag, S M Shafiul Alam

Changing the World's Energy Future

INL is a U.S. Department of Energy National Laboratory operated by Battelle Energy Alliance, LLC

INL/CON-23-75479-Revision-0

Investigating Oscillations in Bulb Turbine Plant During Islanded black start Operation

Soumyadeep Nag, S M Shafiul Alam

October 2024

Idaho National Laboratory
Idaho Falls, Idaho 83415

http://www.inl.gov

Prepared for the
U.S. Department of Energy
Under DOE Idaho Operations Office
Contract DE-AC07-05ID14517

Investigating Oscillations in Bulb Turbine Plant During Islanded Black Start Operation

Soumyadeep Nag, S M Shafiul Alam
Power & Energy Systems, Idaho National Laboratory
Idaho, USA
soumyadeep.nag@inl.gov, smshafiul.alam@inl.gov

***Abstract*—This paper investigates the frequency oscillations displayed by a bulb turbine-based run-of-river (ROR) hydropower system under islanded operation. From a field test it was observed that these oscillations grow as the generator loading increases. These oscillations prevent higher loading of these generators (under islanded conditions) and hence reduce the grid restoration capacity for these individual generators. To investigate the problem, first, a transfer function model of the bulb-turbine system, sensitive to the effects of head variation, blade angle, and other non-linearities pertaining to turbine characteristics is derived. Next, by analyzing this transfer function model and by simulations, it is found that system inertia, hydrogovernor derivative filter time constant, and hydroturbine's unobserved damping and friction are among factors that are responsible for these oscillations. Also, through simulations it is shown that the same ROR system with same controls is non-oscillatory under grid connected condition but oscillates when islanded.**

***Index Terms*—Hydropower, Oscillation, Run-of-river, Black start**

I. Introduction

River-side communities with available ROR resources connected to the distribution network can achieve higher resilience to black-outs with the black start capabilities of these ROR systems. Although this sounds feasible, certain modifications need to be made to the non-black start ROR plant before it can be used as a black start resource. For example, the droop is set to 0%, connection to a "dead" bus is enabled, and frequency protection settings are relaxed. Even after these changes are made, certain problems exist, as discussed below, that are investigated in this paper.

A. Problem Statement

In [1], a series of tests were performed to realize the black start potential of an actual ROR plant that was not initially intended to operate as a black start. Contextually similar efforts can be seen in [2], [3]. Additionally, in [1], a single-plant with and without ultracapacitor (UC) and multi-plant with and without UC test scenarios were examined. As the islanded ROR plant (without any UC) is gradually loaded in steps, the following phenomena are observed: (a) frequency nadir decreases with consecutive load steps (b) frequency oscillation increases as load or operating point increases and (c) the duration spent at lower frequencies increases as load or operating point increases. Due to these problems, the load-carrying capacity of the ROR plant during islanded operation is limited. The aim here is to arrive at reasonable explanations of these issues.

Authored by Battelle Energy Alliance, LLC under Contract No. DE-AC07-05ID14517 with the U.S. Department of Energy (DOE). Work supported through the DOE Water Power Technology Office HydroWIRES Initiative.

B. Literature review

In [4], the IEEE working group on prime movers and energy supply models for the system dynamic performance studies, provided the dynamic models for the hydro turbine and governor models. They considered aspects like the elasticity of the water column, traveling wave effect, surge tank effect, and multiple penstock effect, while also considering permanent droop, proportional-integral (PI), and proportional-integral-derivative (PID) controllers. However, the transfer function that was provided in [4] does not consider the effect of operating head or turbine blade positions.

Based on the model provided in [4], in [5] the authors develop a generalized guide for optimum adjustment of the PID governor gains and other parameters. In [6], a procedure for obtaining the parameters of the non-linear non-elastic penstock and multi-turbine model is presented. The main finding from [6] was that the model as is, is incapable of representing the dynamics accurately and that additional modifications are required. The above-mentioned shortcomings have strongly motivated this work.

In [7], the H6E governor model and an initialization routine are presented in detail. Also, the "grid-connected mode" dynamic performance of the simulation model is matched with field data to derive the parameters of the model. This matched model is used for this study. Similar model-matching efforts on bulb turbines can be found in [8], where authors use polynomial fitting to identify blade and gate functions for the required power, and particle swarm optimization to identify other model parameters from field data.

In the context of oscillations, in [10], the authors show that .05 Hz oscillations in system frequency can be observed in hydro-dominated power networks. The authors have strongly advised that feed-forward controllers should not be used in systems with primary frequency control. In [11] oscillations were found under grid-connected mode that arose from a faulty runner blade. In [12], the authors develop methods of frequency oscillation damping through exciter and guide vane control. Although [10]–[12] mention hydropower-related

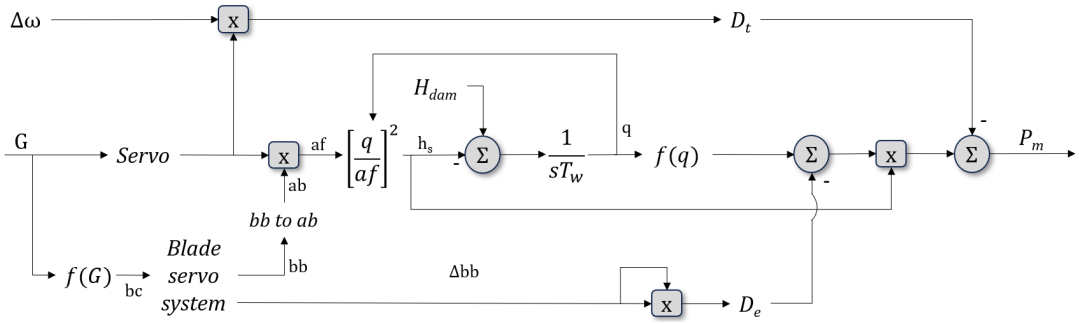

Fig. 1: H6E - Bulb turbine systems functional (alternate representation of [9])

oscillations, none of them address this for islanded operation of bulb turbine system.

Therefore, the aims (and contributions) of this work are to a) arrive at a transfer function model that is sensitive to blade position and operating head variations, but is simultaneously analytical and b) using the derived transfer function, analytically and through simulations, arrive at sensible explanations for the oscillations in [1].

II. System Model

A. Derivation of turbine transfer function considering H_{dam}

Fig. 1 is a simplified form of the standard model available in [9] and [7]. In Fig. 2, the functions $f(q)$ and $f(G)$ are identified as 3^{rd} and 4^{th} order functions as,

$$f(q) = p_{11}q^3 + p_{12}q^2 + p_{13}q + p_{14} \tag{1}$$

and,

$$f(G) = p_{21}G^4 + p_{22}G^3 + p_{23}G^2 + p_{24}G + p_{25} \tag{2}$$

where $\mathbf{p}_1$ and $\mathbf{p}_2$ are vectors of coefficients identified using the polyfit tool of MATLAB [13], and G and q are gate position and flow rate, respectively. The identified curves are shown in Fig. 2 (a) and Fig. 2 (b). The orders of these functions were chosen after a few iterations over the polyfit tool. The iterations were stopped when RMSE reached below 0.025 or there was no significant change in error was recorded.

According to the dynamic model of the turbine and hydraulic system in Fig. 1 the power output from the bulb turbine can be given by:

$$P_m = h_s(f(q) - D_e\Delta bb^2) - GD_t\Delta\omega \tag{3}$$

where $h_s, D_e, D_t, bb, \Delta\omega$, are the dynamic head experienced by the turbine, damping effect of blade change, damping effect turbine speed change, blade opening, and speed deviation, respectively. $\Delta\omega$ and Δbb are defined as $\omega_o - \omega$ and $bb_o - bb$, where subscript o indicates steady - state point of initialization. Assuming that the Δbb and $\Delta\omega$ are 0, we can simplify the above relation as,

$$P_m = h_s f(q). \tag{4}$$

Here,

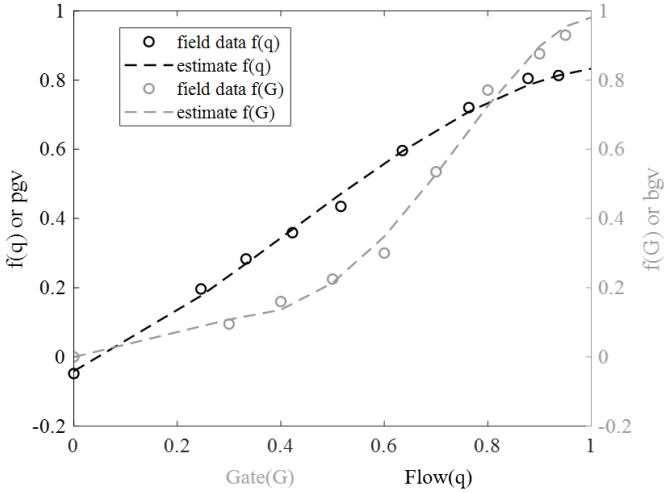

Fig. 2: Curve fitting estimate of (a) power vs. flow and (b) blade vs. gate data obtained from field test [1]

$$h_s = \left(\frac{q}{af}\right)^2 = \left(\frac{q}{ab \times G}\right)^2,$$

and since

$$ab = bb(1 - bgvmin) + bgvmin,$$

assuming $bb = bc = f(G)$, and $k_1 = (1 - bgvmin)$, $k_2 = bgvmin$ we have,

$$P_m = \left\{\frac{q}{G \times [k_1 f(G) + k_2]}\right\}^2 f(q).$$

To generalize with the working group paper [4], and to simplify the analysis that follows, we assume $X = G \times [k_1 f(G) + k_2]$. Therefore, we finally have,

$$P_m = \left(\frac{q}{X}\right)^2 f(q) \tag{5}$$

Using standard Taylor's series as,

$$P_{mo} + \Delta P_m = P_{mo} + \frac{\partial P}{\partial G}\Big|_{q_o,G_o} + \frac{\partial P}{\partial q}\Big|_{q_o,G_o}$$

we linearize (5) around q_o and G_o, to obtain

$$\Delta P_m = \left[\frac{2H_{dam}f(q_o)}{q_o} + H_{dam}f'(q_o)\right]\Delta q - \left[\frac{2H_{dam}f(q_o)A_o}{X_o}\right]\Delta G \quad (6)$$

Here, $A_o = G_o k_1 f'(G_o) + f(G_o)k_1 + k_2$. Under steady-state conditions,

$$H_{dam} = H_o = \left(\frac{q_o}{X_o}\right)^2,$$

where

$$X_o = G_o(f(G_o)k_1 + k_2).$$

The first term on the right-hand side of the (6) is a function of Δq which prevents us from obtaining the form $\frac{\Delta P}{\Delta G}$. The dynamic flow-head equation for the non-elastic non-linear water column is retained as before and is given as

$$\frac{dq}{dt} = \frac{H_o - h_s}{T_w} \quad (7)$$

where T_w is the water time constant of the pipeline. Linearizing equation (7) around G_o and q_o, we get

$$\frac{\Delta q}{\Delta G} = \frac{q_o A_o / X_o}{1 + \frac{sT_w q_o}{2H_o}} \quad (8)$$

In this work, we do not assume that $q_o = X_o$, which would be the case only if $H_o = 1$. Substituting (8) in (6), we finally have

$$\frac{\Delta P_m}{\Delta G} = \frac{C_o(1 - \frac{sT_w D_o}{C_o})}{X_o(1 + \frac{sT_w q_o}{2H_o})} \quad (9)$$

Here

$$B_o = \left[\frac{2H_o f(q_o)}{q_o} + H_o f'(q_o)\right],$$

$$C_o = q_o B_o A_o - 2H_o f(q_o)A_o, \text{ and } D_o = f(q_o)A_o q_o.$$

When a servo is used (as in (12)), ΔG is replaced with $\Delta G'$. The developed transfer function model (9), considering turbine characteristics and non-linearities, is a valuable tool that can be used for power system dynamic analysis and control.

B. Speed Control of the H6E Governor Model

The H6E governor has a load following and a speed regulation mode. As the system under study is islanded, the speed control mode of the H6E governor is considered here. The H6E is basically a PID governor with gate droop in this mode. However, the derivative receives the speed instead of the speed error. Under speed regulation mode the H6E governor takes the shape as shown in Fig. 3.

Here F_1 and F_2 are given as follows:

$$F_1 = \frac{1}{1 + sT_f}; \quad F_2 = \frac{sK_d}{1 + sT_d}.$$

Introducing auxiliary variables e_1 and e_2 we have

$$e_1 = \Delta P^r + \Delta\omega^r - F_1\Delta\omega - R_g e_2$$

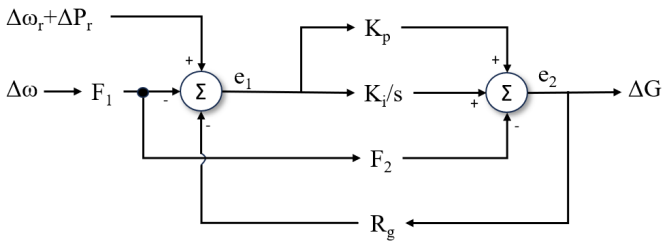

Fig. 3: H6E governor [9]

and

$$e_2 = (K_p + K_i/s)e_1 - F_1F_2\Delta\omega.$$

Assuming $\Delta P_r = 0$ and $\Delta\omega_r = 0$ (as in normal operating conditions), and eliminating e_1 from e_2 and expanding the equations above, we have

$$\frac{\Delta G}{\Delta\omega} = \frac{-K_d}{K_i R_g}\frac{s^2 + K_p/K_d s + K_i/K_d}{[\frac{(1+K_p R_g)}{K_i R_g}s + 1](1 + sT_d)(1 + sT_f)}. \quad (10)$$

Similar to (9), (10) is also an important contribution of this paper. The shaft is considered as

$$\frac{\Delta\omega}{\Delta P} = \frac{1}{D_{sh} + s2H}, \quad (11)$$

where D_{sh} and H are shaft damping and combined generator turbine inertia. The servo mechanism is considered a second-order system as

$$\frac{\Delta G'}{\Delta G} = \frac{K_v}{1 + s + T_v s^2} \quad (12)$$

Here $P_r, \omega_r, K_p, K_i, K_d, T_d, R_g, K_v$, and T_v are the power reference, speed reference, proportional, integral, derivative gains, derivative filter time constant, gate droop, servo gain, and servo time constant.

III. Investigation, Results and Discussion

Reference [1] shows that frequency nadir and oscillations increase with the increase in loading (operating point), which could suggest that,

Hypothesis 1: *the closed loop poles must be gradually moving toward the imaginary axis.*

It should be noted that, hypothesis 1 is based on the f(q) and f(G) dependent transfer function (9), which impact the closed loop poles' proximity to the imaginary axis.

Now, [1] shows that the duration spent at lower frequencies increases as load or operating point increases. Reference [1] also shows that with multiple units online, the time spent below a fixed frequency threshold is comparatively lower than in the case of a single unit, which could suggest that,

Hypothesis 2: *system inertia could be significantly affecting the closed loop poles.*

Finally, with the absence of the grid, and the single ROR plant responsible for maintaining frequency, it could be possible that, compared to the grid-connected condition,

Hypothesis 3: *the effect of dead band, losses, and damping could be more pronounced.*

In what follows, we investigate Hypothesis 1, 2 and 3, and provide possible explanations of the phenomena.

A. Examination of dominant oscillatory poles of the system

The following tables I and II depict the movement of dominant oscillatory poles as the operating point changes. One can easily conclude that as the operating point changes or loading increases, the dominant oscillatory poles move toward the region of instability, which strengthens Hypothesis 1. Furthermore, it is evident that inertia (H) plays an important role in the phenomena since the poles migration toward the unstable region of the s-plane is accelerated, with decreasing inertia. This strengthens Hypothesis 2.

From [1], major controller parameters were confirmed but certain time constants were not revealed. As such the effect of derivative filter time-constant (T_d) is also investigated. From table II, T_d also has a significant effect on the poles. It is observed that as the derivative time-constant is reduced the pole migration toward the unstable region of the s-plane is accelerated.

Although the poles are not yet on the imaginary axis to support sustained oscillations, from the extrapolated trajectory one can comprehend that at a certain amount of loading, these poles would lie on the imaginary axis which would lead to sustained oscillations. Moreover, poles and zeros are found from equations (9), (10), and (12), that consider the linearized model. There could be other non-linearities that accelerate the early onset of oscillations, such as dead bands and saturation effects among others. his motivates a simulation based examination.

TABLE I: Effect of inertia variation and gate opening (operating point) on pole locations with $T_d = 0.05s$

	$H = 1.2s$	$H = 0.6s$	$H = 0.45s$
$G = 0.15pu$	$-3.6 \pm j3.5$	$-2.5 \pm j3.81$	$-1.11 \pm j4.37$
$G = 0.25pu$	$-2.7 \pm j2.28$	$-1.6 \pm j2.71$	$-.17 \pm j3.13$
$G = 0.35pu$	$-2.36 \pm j1.4$	$-1.03 \pm j1.93$	$.31 \pm j2.42$

TABLE II: Effect of derivative time constant variation and gate opening (operating point) on pole locations with $H = 0.6s$

	$T_d = 0.25s$	$T_d = 0.5s$
$G = 0.15pu$	$-1.6 \pm j2.87$	$-1.36 \pm j2.24$
$G = 0.25pu$	$-0.88 \pm j2.22$	$-0.66 \pm j1.87$
$G = 0.35pu$	$-0.49 \pm j1.77$	$-0.31 \pm j1.56$

B. Simulation-based examination of the system

1) System description: The mechanical system consists of a single bulb turbine governor model (H6E [9]) as described by Fig. 1 rated at 8.9MVA and its governor. The electrical system consists of the alternator (at 4.16kV and 38 pole pairs), ST1A excitation system [14], a pair of transformers (one step-up transformer (4.16kV to 46kV), and a step-down transformer (46kV to 12.47kV)) with a short line segment of 700m in between and load bank (at 12.47kV).

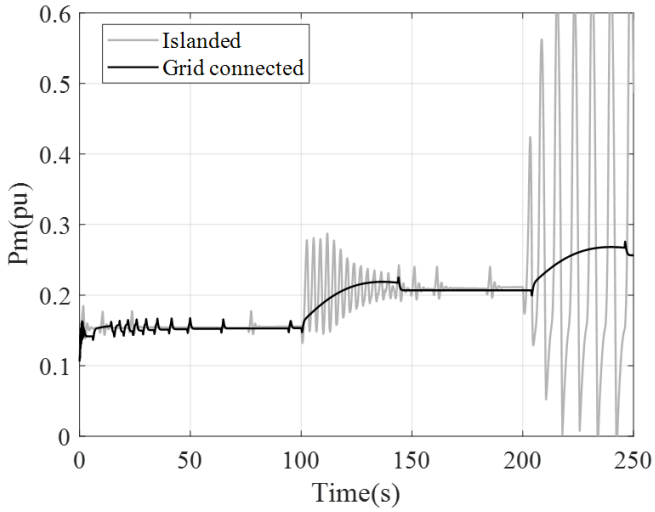

Fig. 4: Comparison of grid-connected behavior and islanded mode behavior

To highlight the problem at hand, we first compare the performance of the same system under grid-connected and islanded mode while retaining the same governor structure and operating conditions.

2) simulation result summary: The islanded mode operation uses the speed control mode of the H6E governor system. For the grid-connected mode, the same speed control mode has been retained but with an additional speed droop function to perform power injection (for the sake of comparison). The system under both modes is loaded from 0.15 pu to 0.25 pu. In islanded mode, load is increased in 0.05 pu increment. It is evident from the results that even with no change in the governor structure when the system is grid-connected it displays no such oscillatory behavior.

Another key point to note is the effect of deadband, turbine damping, and friction, which are not visible through pole-zero analysis. Here, we draw attention towards apparently small blips in mechanical power away from the regions of major oscillations. In the absence of the aid from the grid to remain synchronized, as the system enters the dead band, friction and turbine damping cause the system to deviate out of the dead band. This activates the governor to act. This chain of action produces these small blips. These blips are present in grid-connected mode but die out after a significant amount of time. However, in the case of islanded mode, these reappear(see Fig. 4). This observation strengthens hypothesis 3.

Next, we look at the effect of parameters H and T_d under islanded conditions. From Fig. 5, (a) and (b) we observe the effect of change in inertia. The same change in load of 0.5 MW is applied around the 1 MW initial load point. This

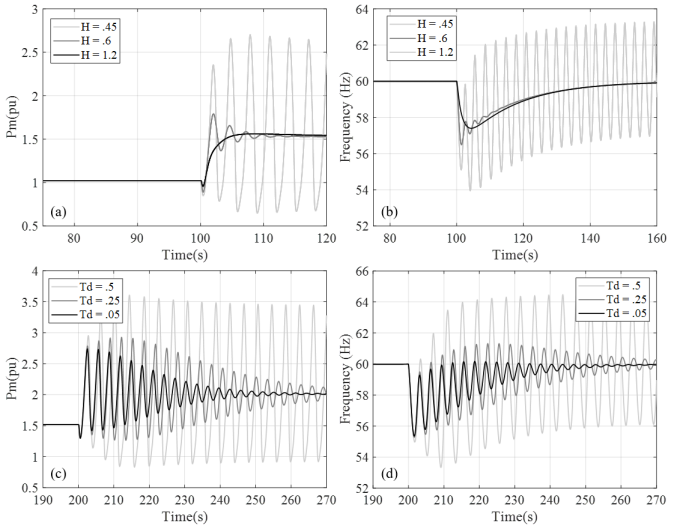

Fig. 5: Effect of change in inertia H (in (a) mechanical power and (b) frequency) and change in derivative filter time constant T_d (in (c) mechanical power and (d) frequency)

strengthens the conclusion from the Table. I that with a higher inertia system has higher load carrying capability during black start. This can also be corroborated with the multi-unit results from [1]. As mentioned before, T_d was one parameter that the field trials did not conclusively state and hence was assumed and thus chosen for examination. From Fig. 5, (c) and (d) we observe the effect of change in derivative filter time constant. The same change in load of 0.5 MW is applied around the 1.5 MW initial load point. This strengthens the conclusion from the Table. II that with a higher T_d the islanded hydropower system's load carrying capability decreases during black start.

On the same note, a separate time - domain simulation of the system in (9) revealed that the undershoot of reverse response (as identified in [4]) increases with operating point. This directly affects the frequency nadir, because the mechanical system absorbs power when the speed drops initially, thereby increasing the frequency nadir as loading increases.

IV. Conclusions

A field test of black start capabilities of local ROR plants was reported in [1], wherein certain problems were identified as stated in section I-A. This work investigates those problems and presents the conclusions of the investigations.

In this paper, a linearized model of the H6E governor turbine has been systematically derived. The derived system is then examined to understand the movement of poles with the change in operating point as system inertia and hydrogovernor's derivative filter time constant are varied. The pole analysis reveals that (a) as the operating point or loading increased, the system's dominant oscillatory poles would move toward the unstable region of the s-plane, and (b) this phenomenon would be boosted by lower inertia or higher derivative filter time constant. These conclusions are also verified by transient simulations. Future work will focus on the comparison of black start and load carrying ability under different operating conditions of head and blade, and across different hydroturbine types.

References

[1] S. Shafiul Alam, R. Bhattarai, T. Hussain, V. Gevorgian, S. Shah, Y. Velaga, M. Roberts, T. Mosier, J. Alzamora, B. Jenkins, and P. Koralewicz, "Enhancing Local Grid Resilience with Small Hydropower Hybrids: Proving the concept through demonstration, simulation, and analysis with Idaho Falls Power," Tech. Rep. INL/RPT-22-69038-Rev000, 1891110, Sep. 2022. [Online]. Available: https://www.osti.gov/servlets/purl/1891110/

[2] B. Jenkins, M. Panwar, and R. Hovsapian, "Experiences from Field Testing for Black Start of a Run-of-the-river Hydropower Plant in Idaho Falls Power Distribution Grid," 2019.

[3] S. M. Shafiul Alam, A. Banerjee, C. Loughmiller, B. D. Bennett, N. Smith, T. M. Mosier, V. Gevorgian, B. Jenkins, and M. Roberts, "Idaho falls power black start field demonstration (preliminary outcomes paper)," 4 2021. [Online]. Available: https://www.osti.gov/biblio/1817907

[4] W. G. P. Mover and E. Supply, "Hydraulic turbine and turbine control models for system dynamic studies," *IEEE Transactions on Power Systems*, vol. 7, no. 1, pp. 167–179, Feb. 1992, conference Name: IEEE Transactions on Power Systems. [Online]. Available: https://ieeexplore.ieee.org/document/141700?denied=

[5] S. Hagihara, H. Yokota, K. Goda, and K. Isobe, "Stability of a Hydraulic Turbine Generating Unit Controlled by P.I.D. Governor," *IEEE Transactions on Power Apparatus and Systems*, vol. PAS-98, no. 6, pp. 2294–2298, Nov. 1979, conference Name: IEEE Transactions on Power Apparatus and Systems. [Online]. Available: https://ieeexplore.ieee.org/document/4113747

[6] L. Hannett, J. Feltes, and B. Fardanesh, "Field tests to validate hydro turbine-governor model structure and parameters," *IEEE Transactions on Power Systems*, vol. 9, no. 4, pp. 1744–1751, Nov. 1994, conference Name: IEEE Transactions on Power Systems. [Online]. Available: https://ieeexplore.ieee.org/document/331426

[7] A. Banerjee, S. M. S. Alam, T. M. Mosier, and J. Undrill, "Modeling a Bulb-Style Kaplan Unit Hydrogovernor and Turbine in Mathworks-Simulink and RTDS-RSCAD," in *2022 IEEE/PES Transmission and Distribution Conference and Exposition (T&D)*. New Orleans, LA, USA: IEEE, Apr. 2022, pp. 1–5. [Online]. Available: https://ieeexplore.ieee.org/document/9816952/

[8] J. Zhao, L. Wang, Y. Tang, D. Liu, and W. Sun, "Hydro Turbine Nonlinear Model Parameter Identification Based on Improved Biogeography-Based Optimization," *Applied Mechanics and Materials*, vol. 672-674, pp. 1617–1621, Oct. 2014.

[9] Powerworld. Governor model: H6e. [Online]. Available: https://www.powerworld.com

[10] H. Villegas Pico, J. D. McCalley, A. Angel, R. Leon, and N. J. Castrillon, "Analysis of Very Low Frequency Oscillations in Hydro-Dominant Power Systems Using Multi-Unit Modeling," *IEEE Transactions on Power Systems*, vol. 27, no. 4, pp. 1906–1915, Nov. 2012, conference Name: IEEE Transactions on Power Systems. [Online]. Available: https://ieeexplore.ieee.org/document/6177295

[11] M. Brezovec, I. Kuzle, M. Krpan, and N. Holjevac, "Improved dynamic model of a bulb turbine-generator for analysing oscillations caused by mechanical torque disturbance on a runner blade," *International Journal of Electrical Power & Energy Systems*, vol. 119, p. 105929, Jul. 2020. [Online]. Available: https://www.sciencedirect.com/science/article/ pii/S0142061519315844

[12] D. Dobrijevic and M. Jankovic, "An improved method of damping of generator oscillations," *IEEE Transactions on Energy Conversion*, vol. 14, no. 4, pp. 1624–1629, Dec. 1999. [Online]. Available: http://ieeexplore.ieee.org/document/815115/

[13] Mathworks. polyfit: Polynomial curve fitting. [Online]. Available: https://www.mathworks.com/help/matlab/ref/polyfit.html

[14] ——. St1a excitation system. [Online]. Available: https://www.mathworks.com/help/sps/powersys/ref/st1aexcitationsystem.html